

Using Pantheon and DES supernova, baryon acoustic oscillation, and Hubble parameter data to constrain the Hubble constant, dark energy dynamics, and spatial curvature

Shulei Cao,^{1*} Joseph Ryan,^{1†} Bharat Ratra^{1‡}

¹Department of Physics, Kansas State University, 116 Cardwell Hall, Manhattan, KS 66502, USA

Accepted XXX. Received YYY; in original form ZZZ

ABSTRACT

We use Pantheon Type Ia supernova (SN Ia) apparent magnitude, DES-3yr binned SN Ia apparent magnitude, Hubble parameter, and baryon acoustic oscillation measurements to constrain six spatially flat and non-flat cosmological models. These sets of data provide mutually consistent cosmological constraints in the six cosmological models we study. A joint analysis of these data sets provides model-independent estimates of the Hubble constant, $H_0 = 68.8 \pm 1.8 \text{ km s}^{-1} \text{ Mpc}^{-1}$, and the non-relativistic matter density parameter, $\Omega_{m0} = 0.294 \pm 0.020$. Although the joint constraints prefer mild dark energy dynamics and a little spatial curvature, they do not rule out dark energy being a cosmological constant and flat spatial hypersurfaces. We also add quasar angular size and H II starburst galaxy measurements to the combined data set and find more restrictive constraints.

Key words: cosmological parameters – dark energy – cosmology: observations

1 INTRODUCTION

That the Universe is currently in a phase of accelerated expansion is well-supported by observations but not fully explained by fundamental theory (see e.g. Ratra & Vogeley 2008; Martin 2012; Coley & Ellis 2020). The standard spatially flat Λ CDM model (Peebles 1984) interprets this phenomenon as a consequence of dark energy with negative pressure (a cosmological constant, Λ) and requires the major part of the energy budget of the Universe to consist of time-independent dark energy and cold dark matter (CDM). Although flat Λ CDM is consistent with many observations (see e.g. Farooq et al. 2017; Scolnic et al. 2018; Planck Collaboration 2020; eBOSS Collaboration 2020),¹ there exist some potential observational discrepancies (Riess 2019; Martinelli & Tutzus 2019) and theoretical puzzles (e.g., Martin 2012), which leaves room for other cosmological models, including non-flat Λ CDM. As the quality and quantity of observational data grow in time, constraining these models is within reach. Many workers have investigated the merits

of the flat and non-flat XCDM parametrizations and ϕ CDM models, where dark energy dynamics and spatial curvature come into play.^{2,3}

Many observational data sets have been used to place constraints on the parameters of cosmological models, such as the equation of state parameter (w) of dark energy. Most recently, in Cao et al. (2021), we used Hubble parameter ($H(z)$), baryon acoustic oscillation (BAO), quasar angular size (QSO), quasar X-ray and UV flux, H II starburst galaxy (H IIIG), and gamma-ray burst (GRB) data to constrain this

² For observational constraints on spatial curvature see Farooq et al. (2015), Chen et al. (2016), Rana et al. (2017), Ooba et al. (2018a,b,c), Yu et al. (2018), Park & Ratra (2018, 2019a,c, 2020), Wei (2018), DES Collaboration (2019a), Handley (2021), Jesus et al. (2021), Li et al. (2020), Geng et al. (2020), Kumar et al. (2021), Efstathiou & Gratton (2020), Di Valentino et al. (2021), Di Valentino et al. (2020), Gao et al. (2020), Abbassi & Abbassi (2020), Yang & Gong (2020), Agudelo Ruiz et al. (2020), Velásquez-Toribio & Fabris (2020), Vagnozzi et al. (2020, 2021), and references therein.

³ For observational constraints on the ϕ CDM model see Yashar et al. (2009), Samushia et al. (2010), Campanelli et al. (2012), Avsajanishvili et al. (2015), Solà et al. (2017), Solà Peracaula et al. (2018, 2019), Zhai et al. (2017), Ooba et al. (2018b, 2019), Sangwan et al. (2018), Singh et al. (2019), Khadka & Ratra (2020a,b,c, 2021), Ureña-López & Roy (2020), and references therein.

* E-mail: shulei@phys.ksu.edu

† E-mail: jwryan@phys.ksu.edu

‡ E-mail: ratra@phys.ksu.edu

¹ Note that the *Planck* TT,TE,EE+lowE+lensing data favor positive spatial curvature (Planck Collaboration 2020) but are consistent with a spatially flat model at 1.63σ .

parameter (among others). The tightest constraints on w , we found, come from low-redshift $H(z)$ (cosmic chronometer) and BAO (standard ruler) data, with the standard candle data (H II G and GRB) giving very broad constraints. In this paper we combine measurements of the distances to 1255 Type Ia supernovae (SNe Ia) with our set of $H(z)$ and BAO data (along with QSO and H II G observations) to obtain tight cosmological parameter constraints.

The usefulness of SN Ia data to cosmology is well-known. SN Ia measurements revealed the accelerated expansion of the Universe over twenty years ago, and they are employed today to place constraints on cosmological parameters and to break parameter degeneracies. Over this time period, the sample size of SN Ia distance measurements has grown considerably, and the analysis and mitigation of systematic uncertainties has improved (DES Collaboration 2019c,d). Supernovae are therefore a reasonably empirically well-understood cosmological probe,⁴ and so can be used to obtain reliable constraints on cosmological model parameters.

In our earlier studies that made use of BAO data (e.g., Ryan et al. 2019; Cao et al. 2021), we relied on CMB-derived values of the baryon density⁵ $\Omega_{b0}h^2$ in order to compute the size of the sound horizon r_s . The size of the sound horizon is needed to calibrate the BAO scale (see Table 1), so the constraints we derived from our BAO measurements were indirectly dependent on CMB physics. Park & Ratra (2018, 2019a,c) computed $\Omega_{b0}h^2$ within each of the six models we study (namely flat/non-flat Λ CDM, flat/non-flat XCDM, and flat/non-flat ϕ CDM) from CMB data using primordial energy density fluctuation power spectra $P(k)$ appropriate for flat and curved geometries (Lucchin & Matarrese 1985; Ratra 1989, 2017; Ratra & Peebles 1995). Other power spectra have been considered in the non-flat case (Lesgourgues & Tram 2014; Bonga et al. 2016; Handley 2019; Thavanesan et al. 2021). Since we do not make use of $P(k)$, the controversy associated with $P(k)$ in non-flat models is avoided in our analyses here.

The constraints from $H(z) + \text{BAO}$ data and from SN Ia data are not inconsistent, and so these data can be jointly used to constrain cosmological parameters. Park & Ratra (2019b) used $H(z)$, BAO, and Pantheon SN Ia apparent magnitude (SN-Pantheon) measurements in such a joint analysis. Here we use a more recent BAO data compilation and new DES-3yr binned SN Ia apparent magnitude (SN-DES) data. We find for all combinations of data we study here that all or almost all of the favored parameter space corresponds to currently accelerating cosmological expansion. The most reliable constraints come from the $H(z) + \text{BAO} + \text{SN-Pantheon} + \text{SN-DES}$ (HzBSNPD) data combination, with fairly model-independent determinations of the Hubble constant, $H_0 = 68.8 \pm 1.8 \text{ km s}^{-1} \text{ Mpc}^{-1}$, and the non-relativistic matter density parameter, $\Omega_{m0} = 0.294 \pm 0.020$. The estimate of H_0 is in better agreement with the median statistics $H_0 = 68 \pm 2.8 \text{ km s}^{-1} \text{ Mpc}^{-1}$ estimate of Chen

⁴ Though the relatively simpler physics underlying cosmic microwave background (CMB) anisotropies and BAO makes those probes better understood than SNe Ia.

⁵ Here Ω_{b0} is the baryon density parameter and $h = H_0/(100 \text{ km s}^{-1} \text{ Mpc}^{-1})$.

& Ratra (2011) and the Planck Collaboration (2020) estimate of $H_0 = 67.4 \pm 0.5 \text{ km s}^{-1} \text{ Mpc}^{-1}$ than with the local $H_0 = 74.03 \pm 1.42 \text{ km s}^{-1} \text{ Mpc}^{-1}$ measurement of Riess et al. (2019). The combined measurements are consistent with the spatially flat Λ CDM model, but also favor some dark energy dynamics, as well as a little non-zero spatial curvature energy density. More restrictive constraints are derived when these data are combined with QSO and H II G data.

This paper is organized as follows. Section 2 summarizes the models we analyze. In Section 3 the data used are introduced and our method of analyzing these data is described in Section 4. We present our results in Section 5, and our conclusions in Section 6.

2 COSMOLOGICAL MODELS

We seek to obtain constraints on the parameters of the flat and non-flat Λ CDM, XCDM, and ϕ CDM models and to compare how well these models fit the observations we study. These models have been described in Ryan et al. (2019) and Cao et al. (2021); see those papers for more details. Our approach here differs from that of those earlier papers in that, instead of varying the non-relativistic matter density parameter Ω_{m0} as a free parameter, we vary the baryonic ($\Omega_{b0}h^2$) and cold dark matter ($\Omega_{c0}h^2$) densities as free parameters, treating Ω_{m0} as a derived parameter.⁶

The expansion rate function $E(z) \equiv H(z)/H_0$ takes the following form in the non-flat Λ CDM model:

$$E(z) = \sqrt{\Omega_{m0}(1+z)^3 + \Omega_{k0}(1+z)^2 + \Omega_\Lambda}, \quad (1)$$

where z is the redshift,

$$\Omega_{m0} = \frac{\Omega_{b0}h^2 + \Omega_{c0}h^2}{h^2} + \Omega_{\nu0}, \quad (2)$$

and

$$\Omega_\Lambda = 1 - \Omega_{m0} - \Omega_{k0}. \quad (3)$$

Ω_{k0} is the curvature energy density parameter, and $\Omega_{\nu0}$ is the neutrino energy density parameter, which we, following Carter et al. (2018), set to $\Omega_{\nu0} = 0.0014$ for all models. The non-flat Λ CDM model therefore has four free parameters: h , $\Omega_{b0}h^2$, $\Omega_{c0}h^2$, and Ω_{k0} . The flat Λ CDM model is a special case with $\Omega_{k0} = 0$.

In the non-flat XCDM parametrization, the expansion rate function takes the form

$$E(z) = \sqrt{\Omega_{m0}(1+z)^3 + \Omega_{k0}(1+z)^2 + \Omega_{X0}(1+z)^{3(1+w_X)}}, \quad (4)$$

where

$$\Omega_{X0} = 1 - \Omega_{m0} - \Omega_{k0}. \quad (5)$$

Here w_X is the equation of state parameter of the X-fluid. The non-flat XCDM parametrization therefore has five free parameters: h , $\Omega_{b0}h^2$, $\Omega_{c0}h^2$, Ω_{k0} , and w_X . The flat XCDM parametrization is a special case in which $\Omega_{k0} = 0$.

⁶ We do this to eliminate the dependence of the BAO data on CMB physics; see Section 3 for details.

In the non-flat ϕ CDM model (Peebles & Ratra 1988; Ratra & Peebles 1988; Pavlov et al. 2013), a scalar field ϕ plays the role of a time-varying cosmological ‘‘constant’’. The expansion rate function in this model takes the form

$$E(z) = \sqrt{\Omega_{m0}(1+z)^3 + \Omega_{k0}(1+z)^2 + \Omega_\phi(z, \alpha)}, \quad (6)$$

where the energy density parameter of the scalar field ϕ , $\Omega_\phi(z, \alpha)$, is determined by numerically integrating the scalar field’s equations of motion. In this quantity α is the parameter that controls the shape of the inverse power law potential energy density $V(\phi)$ of ϕ .⁷ The non-flat ϕ CDM model therefore has five free parameters: h , $\Omega_{b0}h^2$, $\Omega_{c0}h^2$, Ω_{k0} , and α . The flat ϕ CDM model is a special case in which $\Omega_{k0} = 0$.

3 DATA

In this paper, we use a combination of $H(z)$, BAO, SN-Pantheon, SN-DES, QSO, and H II G data to constrain the cosmological models we study.

The $H(z)$ data, compiled in Table 2 of Ryan et al. (2018), consist of 31 measurements spanning the redshift range $0.070 \leq z \leq 1.965$. The BAO data, which have been updated relative to Cao et al. (2020), consist of 11 measurements spanning the redshift range $0.38 \leq z \leq 2.334$, listed in Table 1.

The SN-Pantheon data, compiled by Scolnic et al. (2018), consist of 1048 SN Ia measurements spanning the redshift range $0.01 < z < 2.3$. The SN-DES data, compiled by DES Collaboration (2019d), consist of 20 binned measurements of 207 SN Ia measurements spanning the redshift range $0.015 \leq z \leq 0.7026$.

The QSO data, listed in Table 1 of Cao et al. (2017), consist of 120 measurements of the angular size

$$\theta(z) = \frac{l_m}{D_A(z)}, \quad (7)$$

spanning the redshift range $0.462 \leq z \leq 2.73$. l_m is the characteristic linear size of the quasars in the sample. This quantity is determined by using the Gaussian Process method to reconstruct the expansion history of the Universe from 24 cosmic chronometer measurements over $z < 1.2$. This $H(z)$ function is used to reconstruct the angular size distance $D_A(z)$, which can then be used to compute l_m given measurements ($\theta_{\text{obs}}(z)$) of quasar angular sizes. QSO and $H(z)$ data are therefore somewhat correlated, but the error bars on the constraints derived from QSO data are so large that we do not believe this correlation to be an issue.

The H II G data consist of 107 low redshift ($0.0088 \leq z \leq 0.16417$) measurements, used in Chávez et al. (2014) (recalibrated by González-Morán et al. 2019), and 46 high redshift ($0.636427 \leq z \leq 2.42935$) measurements.

The covariance matrix \mathbf{C} for the BAO data, taken from Alam et al. (2017), is given in equation (20) of Ryan et al. (2019). For the BAO data from du Mas des Bourboux et al. (2020), the covariance matrix is

$$\mathbf{C} = \begin{bmatrix} 1.3225 & -0.1009 \\ -0.1009 & 0.0380 \end{bmatrix}. \quad (8)$$

⁷ The details of this model are described in Cao et al. (2020, 2021).

Table 1. BAO data.

z	Measurement ^a	Value	Ref.
0.38	$D_M(r_{s,\text{fid}}/r_s)$	1512.39	Alam et al. (2017) ^b
0.38	$H(z)(r_s/r_{s,\text{fid}})$	81.2087	Alam et al. (2017) ^b
0.51	$D_M(r_{s,\text{fid}}/r_s)$	1975.22	Alam et al. (2017) ^b
0.51	$H(z)(r_s/r_{s,\text{fid}})$	90.9029	Alam et al. (2017) ^b
0.61	$D_M(r_{s,\text{fid}}/r_s)$	2306.68	Alam et al. (2017) ^b
0.61	$H(z)(r_s/r_{s,\text{fid}})$	98.9647	Alam et al. (2017) ^b
0.122	$D_V(r_{s,\text{fid}}/r_s)$	539 ± 17	Carter et al. (2018)
0.81	D_A/r_s	10.75 ± 0.43	DES Collaboration (2019b)
1.52	$D_V(r_{s,\text{fid}}/r_s)$	3843 ± 147	Ata et al. (2018)
2.334	D_M/r_s	37.5	du Mas des Bourboux et al. (2020) ^c
2.334	D_H/r_s	8.99	du Mas des Bourboux et al. (2020) ^c

^a D_M , D_V , r_s , $r_{s,\text{fid}}$, D_A , and D_M have units of Mpc, while $H(z)$ has units of $\text{km s}^{-1} \text{Mpc}^{-1}$.

^b The six measurements from Alam et al. (2017) are correlated; see equation (20) of Ryan et al. (2019) for their correlation matrix.

^c The two measurements from du Mas des Bourboux et al. (2020) are correlated; see equation (8) below for their correlation matrix.

The scale of BAO measurements is set by the sound horizon (r_s) during the epoch of radiation drag. To compute this quantity, we use the approximate formula (Aubourg et al. 2015)

$$r_s = \frac{55.154 \exp[-72.3(\Omega_{b0}h^2 + 0.0006)^2]}{(\Omega_{b0}h^2)^{0.12807}(\Omega_{c0}h^2 + \Omega_{b0}h^2)^{0.25351}} \text{Mpc}. \quad (9)$$

In our previous studies we did not vary $\Omega_{b0}h^2$ as a free parameter. Instead we used CMB-derived, model-dependent values of $\Omega_{b0}h^2$ to compute r_s . Because we vary $\Omega_{b0}h^2$ as a free parameter in this paper, our computations of the sound horizon (and therefore our calibration of the scale of our BAO measurements) are fully independent of CMB physics (at the cost of enlarging the parameter space and so somewhat weakening the constraints).

Following Conley et al. (2011) and Deng & Wei (2018), we define the theoretical magnitude of a supernova to be

$$m_{\text{th}} = 5 \log \mathcal{D}_L(z) + \mathcal{M}, \quad (10)$$

where \mathcal{M} is a nuisance parameter to be marginalized over, and $\mathcal{D}_L(z)$ is

$$\mathcal{D}_L(z) \equiv (1 + z_{\text{hel}}) \int_0^{z_{\text{cmb}}} \frac{dz}{E(\tilde{z})}. \quad (11)$$

In this equation, z_{hel} is the heliocentric redshift, and z_{cmb} is the CMB-frame redshift. In Conley et al. (2011), equation (11) is called the ‘‘Hubble-constant free luminosity distance’’, because $E(z)$ does not contain H_0 . In our case, because we use h , $\Omega_{b0}h^2$, and $\Omega_{c0}h^2$ as free parameters, our expansion rate function (and thus our luminosity distance) depends on the Hubble constant. We therefore obtain weak constraints on H_0 from the supernova data, unlike Conley et al. (2011) and Deng & Wei (2018) (see Section 5, below).

4 DATA ANALYSIS METHODOLOGY

We use the PYTHON module EMCEE (Foreman-Mackey et al. 2013) to maximize the likelihood functions, thereby determining the constraints on the free parameters. In our analyses here the priors on the cosmological parameters are different from zero (and flat) over the ranges $0.005 \leq \Omega_{b0}h^2 \leq 0.1$, $0.001 \leq \Omega_{c0}h^2 \leq 0.99$, $0.2 \leq h \leq 1.0$, $-3 \leq w_X \leq 0.2$, $-0.7 \leq \Omega_{k0} \leq 0.7$, and $0 < \alpha \leq 10$. Ω_{m0} is a derived parameter and depends on h .

The likelihood functions of $H(z)$, BAO, H II G, and QSO data are described in Cao et al. (2020) and Cao et al. (2021). For the SN Ia (SN-Pantheon and SN-DES) data, the likelihood function is

$$\mathcal{L}_{\text{SN}} = e^{-\chi_{\text{SN}}^2/2}, \quad (12)$$

where, as in Park & Ratra (2019b), χ_{SN}^2 takes the form of equation (C1) in Appendix C of Conley et al. (2011) with \mathcal{M} being marginalized. The covariance matrices of the SN Ia data, \mathbf{C}_{SN} are the sum of the diagonal statistical uncertainty covariance matrices, $\mathbf{C}_{\text{stat}} = \text{diag}(\sigma_{\text{SN}}^2)$, and the systematic uncertainty covariance matrices, \mathbf{C}_{sys} . $\mathbf{C}_{\text{SN}} = \mathbf{C}_{\text{stat}} + \mathbf{C}_{\text{sys}}$.⁸ σ_{SN} are the SN Ia statistical uncertainties.

As in Cao et al. (2021), we use the Akaike Information Criterion (*AIC*) and the Bayesian Information Criterion (*BIC*) to compare the quality of models with different numbers of parameters, where

$$AIC = -2 \ln \mathcal{L}_{\text{max}} + 2n, \quad (13)$$

and

$$BIC = -2 \ln \mathcal{L}_{\text{max}} + n \ln N. \quad (14)$$

In the preceding equations, \mathcal{L}_{max} , n , and N are the maximum value of the considered likelihood function, the number of free parameters in the given model, and the number of used data points (e.g., for SN-Pantheon $N = 1048$), respectively.

5 RESULTS

The posterior one-dimensional (1D) probability distributions and two-dimensional (2D) confidence regions of the cosmological parameters for the six flat and non-flat models are shown in Figs. 1–6, in gray ($H(z)$ +BAO), red ($H(z)$ + BAO + SN-Pantheon, HzBSNP), green ($H(z)$ + BAO + SN-DES, HzBSND), blue ($H(z)$ + BAO + SN-Pantheon + SN-DES, HzBSNPD), and purple ($H(z)$ + BAO + SN-Pantheon + SN-DES + QSO + H II G, HzBSNPQH). We list the unmarginalized best-fitting parameter values, as well as the corresponding χ^2 , *AIC*, *BIC*, and degrees of freedom ν ($\nu \equiv N - n$) for all models and data combinations, in Table 2. The marginalized best-fitting parameter values and uncertainties ($\pm 1\sigma$ error bars or 2σ limits), for all models and data combinations, are listed in Table 3.⁹

5.1 $H(z)$ + BAO, HzBSNP, and HzBSND constraints

The 1D marginalized $H(z)$ + BAO constraints on the cosmological parameters are listed in Table 3. These are (slightly) different from the ones obtained by Khadka & Ratra (2021), because of the different treatments of both the prior ranges and the coefficient κ in the ϕ CDM models.¹⁰

⁸ Note that the covariance matrices for the SN-DES data are the ones described in equation (18) of DES Collaboration (2019d).

⁹ The PYTHON package GETDIST (Lewis 2019) is used to analyze the samples.

¹⁰ We treated κ as a derived constant determined from the parameter α (see e.g. eq. (14) of Cao et al. 2021), while Khadka & Ratra (2021) treated it as a constant derived from the energy budget equation.

The $H(z)$, BAO, and SN-Pantheon data combinations have previously been studied (Park & Ratra 2019b). Relative to that analysis, we use the updated BAO data, shown in Table 1, in our analysis here. In the HzBSNP case, we find that the determinations of Ω_{k_0} are more consistent with flat spatial hypersurfaces than what Park & Ratra (2019b) found and dark energy dynamics favors less deviation from a cosmological constant in the XCDM cases, while favoring a somewhat stronger deviation from $\alpha = 0$ in the non-flat ϕ CDM case.

Because the $H(z)$, BAO, and SN-DES constraints are consistent across all six of the models we study, we also perform a joint analysis of these data to determine HzBSND constraints. Relative to the HzBSNP constraints, the measured values of $\Omega_{b_0}h^2$, $\Omega_{c_0}h^2$, and Ω_{m_0} are a little higher, lower, and lower (except for flat Λ CDM) than those values measured from the HzBSNP case, respectively. Given the error bars, these differences are not statistically significant. The measured values of H_0 are lower than those for the HzBSNP case. The non-flat XCDM and ϕ CDM models favor more and less closed geometry than in the HzBSNP case. The non-flat Λ CDM model favors more open geometry than in the HzBSNP case. The constraints for all three non-flat models are consistent with spatially flat hypersurfaces. The fits to the HzBSND data produce stronger evidence for dark energy dynamics than the fits to the HzBSNP data.

5.2 HzBSNPD constraints

The results of the previous three subsections show that, when combined with $H(z)$ + BAO data, SN-Pantheon data produce tighter constraints on almost all cosmological parameters, than do SN-DES data (with a few exceptions including $\Omega_{b_0}h^2$ for non-flat Λ CDM, $\Omega_{c_0}h^2$ for non-flat ϕ CDM, and Ω_{m_0} and H_0 for flat and non-flat ϕ CDM). Since the $H(z)$ + BAO, SN-Pantheon, and SN-DES data constraints are not inconsistent, it is useful to derive constraints from an analysis of the combined $H(z)$, BAO, SN-Pantheon, and SN-DES (HzBSNPD) data. The results of such an analysis are presented in this subsection. We discuss these results in some detail here because, as discussed in Sec. 5.4, we believe that the constraints we obtain from the HzBSNPD data combination are more reliable than the constraints we obtain from the other data combinations we study.

The measured values of $\Omega_{b_0}h^2$ range from a low of $0.0241^{+0.0024}_{-0.0030}$ (flat Λ CDM) to a high of $0.0279^{+0.0031}_{-0.0048}$ (flat ϕ CDM) and those of $\Omega_{c_0}h^2$ range from a low of $0.1047^{+0.0125}_{-0.0096}$ (flat ϕ CDM) to a high of 0.1199 ± 0.0067 (flat Λ CDM). The derived constraints on Ω_{m_0} range from a low of $0.284^{+0.017}_{-0.016}$ (flat ϕ CDM) to a high of 0.303 ± 0.013 (flat Λ CDM). These measurements are consistent with what is measured by Planck Collaboration (2020). In particular, for flat Λ CDM, comparing to the TT,TE,EE+lowE+lensing results in Table 2 of Planck Collaboration (2020) the error bars we find here for $\Omega_{b_0}h^2$, $\Omega_{c_0}h^2$, and Ω_{m_0} are a factor of 18, 5.6, and 1.8, respectively, larger than the Planck error bars, and our estimates here for the quantities differ from the Planck estimates by 0.58σ , 0.015σ , and 0.82σ , respectively.

The constraints on H_0 are between $H_0 = 68.48^{+1.71}_{-1.70}$ $\text{km s}^{-1} \text{Mpc}^{-1}$ (flat ϕ CDM) and $H_0 = 69.14 \pm 1.68$ $\text{km s}^{-1} \text{Mpc}^{-1}$ (flat Λ CDM), which are 0.35σ (flat Λ CDM) and 0.15σ (flat ϕ CDM) higher than the median statistics

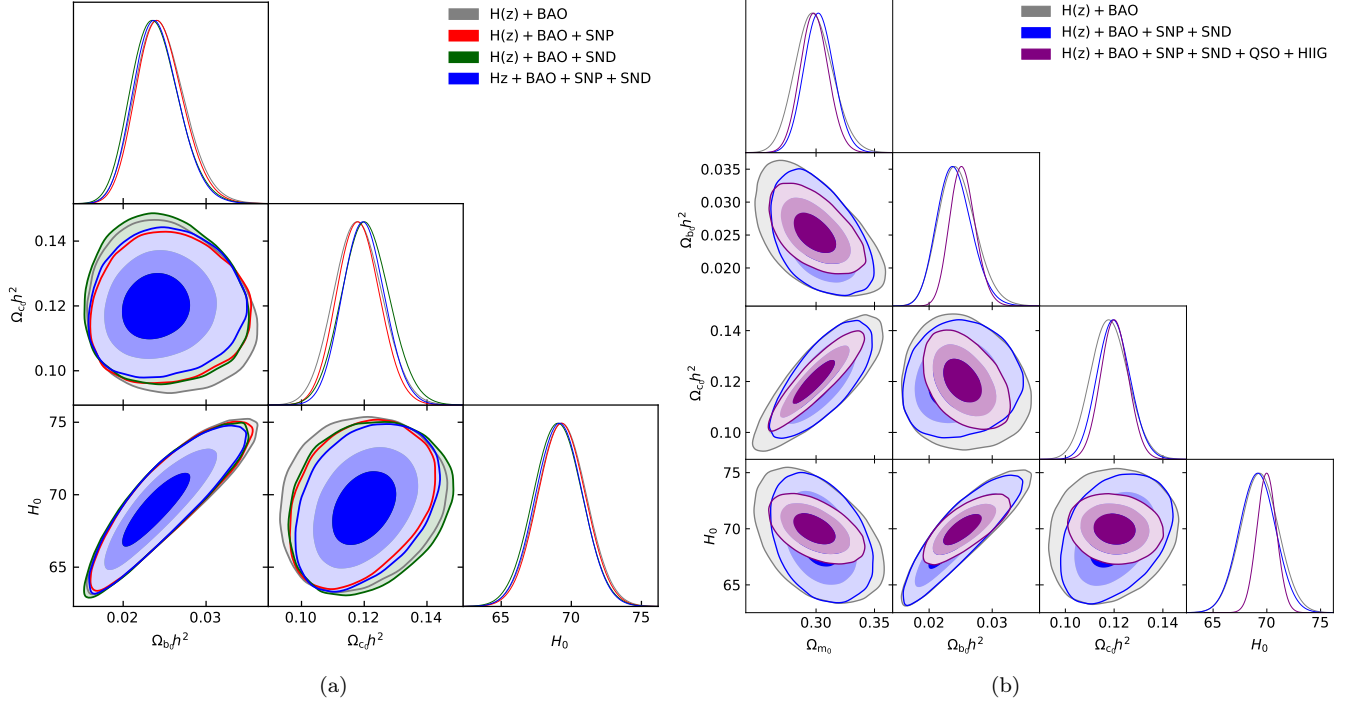


Figure 1. 1σ , 2σ , and 3σ confidence contours for flat Λ CDM, where the right panel is the comparison including derived cosmological matter density parameter Ω_{m0} . In all cases, the favored parameter space is associated with currently-accelerating cosmological expansion.

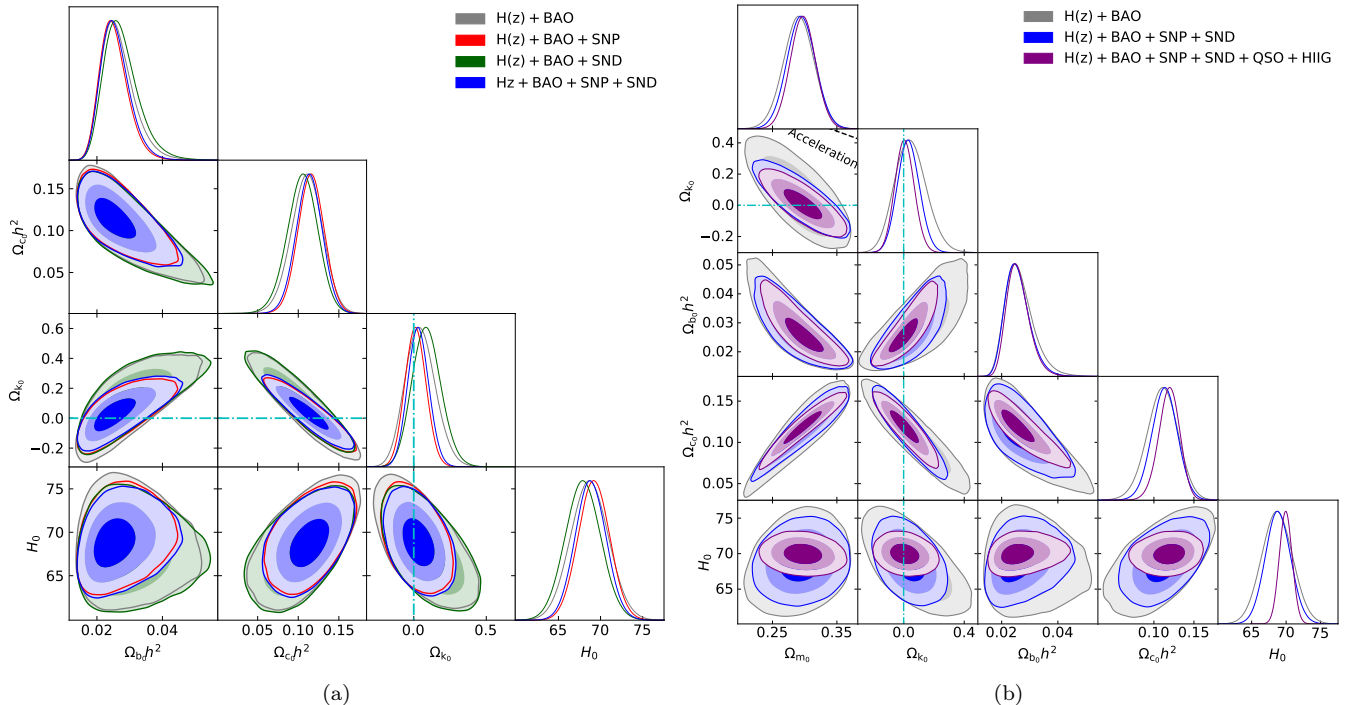


Figure 2. Same as Fig. 1 but for non-flat Λ CDM, where the cyan dash-dot lines represent the flat Λ CDM case, with closed spatial hypersurfaces either below or to the left. The black dotted line in the right subpanel is the zero-acceleration line, which divides the parameter space into regions associated with currently-accelerating (below left) and currently-decelerating (above right) cosmological expansion. In all cases, the favored parameter space is associated with currently-accelerating cosmological expansion.

Table 2. Unmarginalized best-fitting parameter values for all models from various combinations of data.

Model	Data set	$\Omega_{b_0} h^2$	$\Omega_{c_0} h^2$	Ω_{m_0}	Ω_{k_0}	w_X	α	H_0^a	χ^2	ν	AIC	BIC
Flat Λ CDM	$H(z) + \text{BAO}$	0.0240	0.1179	0.299	–	–	–	69.11	23.64	39	29.64	34.86
	HzBSNP ^b	0.0240	0.1180	0.299	–	–	–	69.10	1053.22	1087	1059.22	1074.21
	HzBSND ^c	0.0234	0.1203	0.305	–	–	–	68.82	50.83	59	56.83	63.21
	HzBSNPD ^d	0.0236	0.1196	0.303	–	–	–	68.91	1080.46	1107	1086.46	1101.50
	HzBSNPDQH ^e	0.0251	0.1203	0.299	–	–	–	69.92	1844.99	1380	1850.99	1866.69
Non-flat Λ CDM	$H(z) + \text{BAO}$	0.0248	0.1136	0.294	0.026	–	–	68.75	23.58	38	31.58	38.53
	HzBSNP ^b	0.0241	0.1172	0.298	0.004	–	–	69.06	1053.22	1086	1061.22	1081.20
	HzBSND ^c	0.0258	0.1081	0.292	0.071	–	–	67.92	50.28	58	58.28	66.79
	HzBSNPD ^d	0.0245	0.1150	0.297	0.023	–	–	68.68	1080.35	1106	1088.35	1108.40
	HzBSNPDQH ^e	0.0249	0.1209	0.300	–0.004	–	–	69.93	1844.99	1379	1852.99	1873.92
Flat XCDM	$H(z) + \text{BAO}$	0.0323	0.0860	0.280	–	–0.696	–	65.12	19.65	38	27.65	34.60
	HzBSNP ^b	0.0254	0.1120	0.292	–	–0.951	–	68.72	1052.63	1086	1060.63	1080.61
	HzBSND ^c	0.0300	0.0934	0.286	–	–0.752	–	65.90	45.46	58	53.46	61.97
	HzBSNPD ^d	0.0256	0.1107	0.293	–	–0.932	–	68.43	1079.23	1106	1087.23	1107.28
	HzBSNPDQH ^e	0.0268	0.1136	0.291	–	–0.949	–	69.63	1844.27	1379	1852.27	1873.20
Non-flat XCDM	$H(z) + \text{BAO}$	0.0302	0.0956	0.294	–0.155	–0.650	–	65.55	18.31	37	28.31	37.00
	HzBSNP ^b	0.0234	0.1231	0.307	–0.103	–0.895	–	69.25	1051.82	1085	1061.82	1086.79
	HzBSND ^c	0.0277	0.1046	0.301	–0.136	–0.711	–	66.45	44.34	57	54.34	64.98
	HzBSNPD ^d	0.0236	0.1220	0.307	–0.107	–0.877	–	68.98	1078.36	1105	1088.36	1113.42
	HzBSNPDQH ^e	0.0242	0.1217	0.303	–0.092	–0.900	–	69.54	1843.25	1378	1853.25	1879.41
Flat ϕ CDM	$H(z) + \text{BAO}$	0.0361	0.0758	0.264	–	–	1.484	65.30	19.48	38	27.48	34.43
	HzBSNP ^b	0.0260	0.1145	0.292	–	–	0.101	69.51	1051.46	1086	1059.46	1079.44
	HzBSND ^c	0.0328	0.0860	0.273	–	–	1.061	66.16	45.17	58	53.17	61.68
	HzBSNPD ^d	0.0254	0.1102	0.292	–	–	0.168	68.35	1078.18	1106	1086.18	1106.22
	HzBSNPDQH ^e	0.0264	0.1135	0.290	–	–	0.132	69.57	1842.95	1379	1850.95	1871.88
Non-flat ϕ CDM	$H(z) + \text{BAO}$	0.0354	0.0811	0.269	–0.148	–	1.819	66.06	18.16	37	28.16	36.85
	HzBSNP ^b	0.0234	0.1225	0.305	–0.133	–	0.393	69.32	1050.31	1085	1060.31	1085.28
	HzBSND ^c	0.0319	0.0933	0.282	–0.140	–	1.411	66.84	44.09	57	54.09	64.72
	HzBSNPD ^d	0.0256	0.1159	0.298	–0.080	–	0.377	69.09	1077.13	1105	1087.13	1112.19
	HzBSNPDQH ^e	0.0258	0.1155	0.293	–0.078	–	0.354	69.55	1842.00	1378	1852.00	1878.16

^a km s⁻¹ Mpc⁻¹.^b $H(z) + \text{BAO} + \text{SN-Pantheon}$.^c $H(z) + \text{BAO} + \text{SN-DES}$.^d $H(z) + \text{BAO} + \text{SN-Pantheon} + \text{SN-DES}$.^e $H(z) + \text{BAO} + \text{SN-Pantheon} + \text{SN-DES} + \text{QSO} + \text{H II G}$.

estimate of $H_0 = 68 \pm 2.8$ km s⁻¹ Mpc⁻¹ (Chen & Ratra 2011), and 2.22σ (flat Λ CDM) and 2.50σ (flat ϕ CDM) lower than the local Hubble constant measurement of $H_0 = 74.03 \pm 1.42$ km s⁻¹ Mpc⁻¹ (Riess et al. 2019).¹¹ For flat Λ CDM our H_0 error bar is a factor of 3.1 larger than that

¹¹ Other local expansion rate H_0 measurements result in slightly lower central values with slightly larger error bars (Rigault et al. 2015; Zhang et al. 2017; Dhawan et al. 2018; Fernández Arenas et al. 2018; Freedman et al. 2020; Rameez & Sarkar 2019; Breuval et al. 2020; Efstathiou 2020; Khetan et al. 2021). Our H_0 determinations are consistent with earlier median statistics determinations (Gott et al. 2001; Chen et al. 2003) as well as with other recent H_0 measurements (Chen et al. 2017; DES Collaboration 2018; Gómez-Valent & Amendola 2018; Planck Collaboration 2020; Domínguez et al. 2019; Cuceu et al. 2019; Zeng & Yan 2019; Schöneberg et al. 2019; Lin & Ishak 2019; Blum et al. 2020; Lyu et al. 2020; Philcox et al. 2020; Zhang & Huang 2021; Birrer et al. 2020; Denzel et al. 2021; Pogosian et al. 2020; Boruah et al. 2020; Kim et al. 2020; Harvey 2020).

from the *Planck* data and our H_0 estimate is 1.01σ higher than that of *Planck*.

For non-flat Λ CDM, non-flat XCDM, and non-flat ϕ CDM, we find $\Omega_{k_0} = 0.032 \pm 0.072$, $\Omega_{k_0} = -0.071^{+0.110}_{-0.123}$, and $\Omega_{k_0} = -0.105 \pm 0.104$, respectively, with non-flat ϕ CDM favoring closed geometry at 1.01σ . The non-flat XCDM and ϕ CDM models favor closed geometry, while the non-flat Λ CDM model favors open geometry. The constraints for non-flat Λ CDM and XCDM models are consistent with spatially flat hypersurfaces.

The fits to the HzBSNPD data favor dark energy dynamics, where for flat (non-flat) XCDM, $w_X = -0.932 \pm 0.061$ ($w_X = -0.904^{+0.098}_{-0.058}$), with best-fitting value being 1.11σ (1.66σ) away from $w_X = -1$; and for flat (non-flat) ϕ CDM, $\alpha = 0.320^{+0.108}_{-0.277}$ ($\alpha = 0.509^{+0.212}_{-0.370}$), with best-fitting value being 1.16σ (1.38σ) away from $\alpha = 0$.

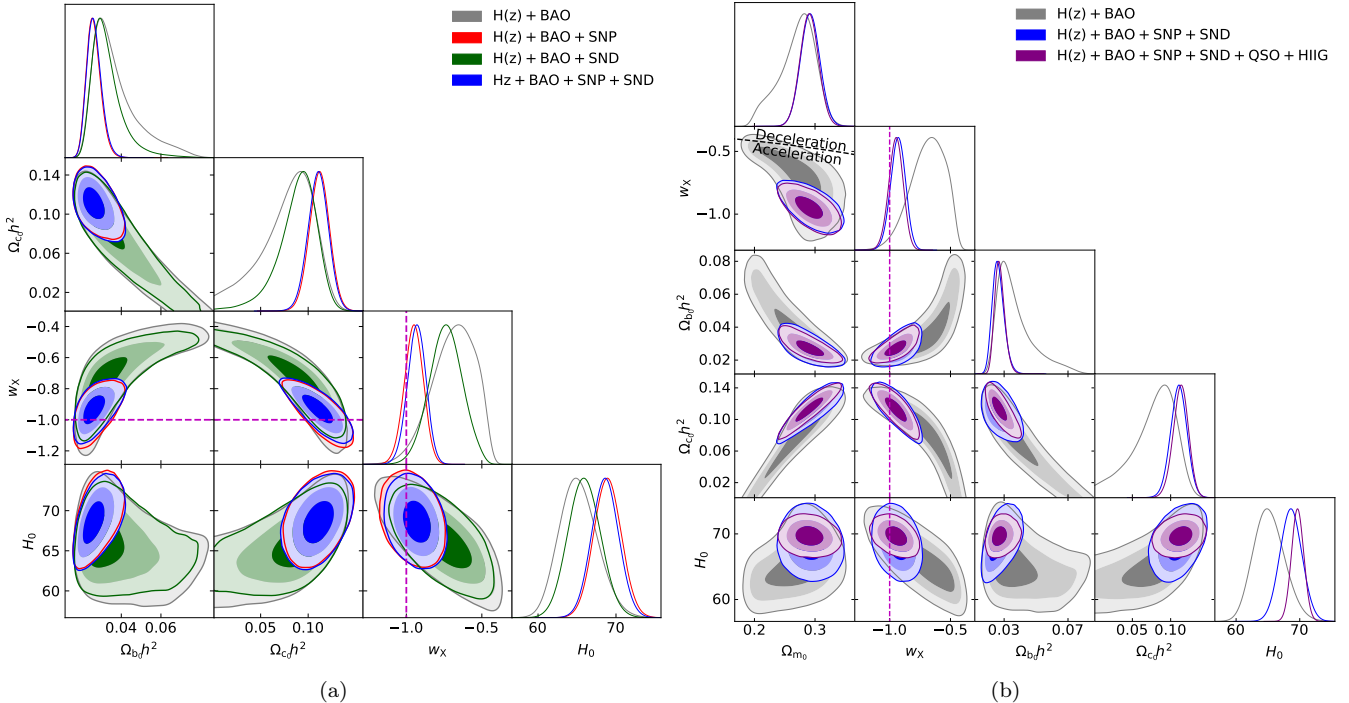


Figure 3. 1σ , 2σ , and 3σ confidence contours for flat XCDM. The black dotted line in the right panel is the zero-acceleration line, which divides the parameter space into regions associated with currently-accelerating (below) and currently-decelerating (above) cosmological expansion. In all cases, almost all of the favored parameter space is associated with currently-accelerating cosmological expansion. The magenta lines denote $w_X = -1$, i.e. the flat Λ CDM model.

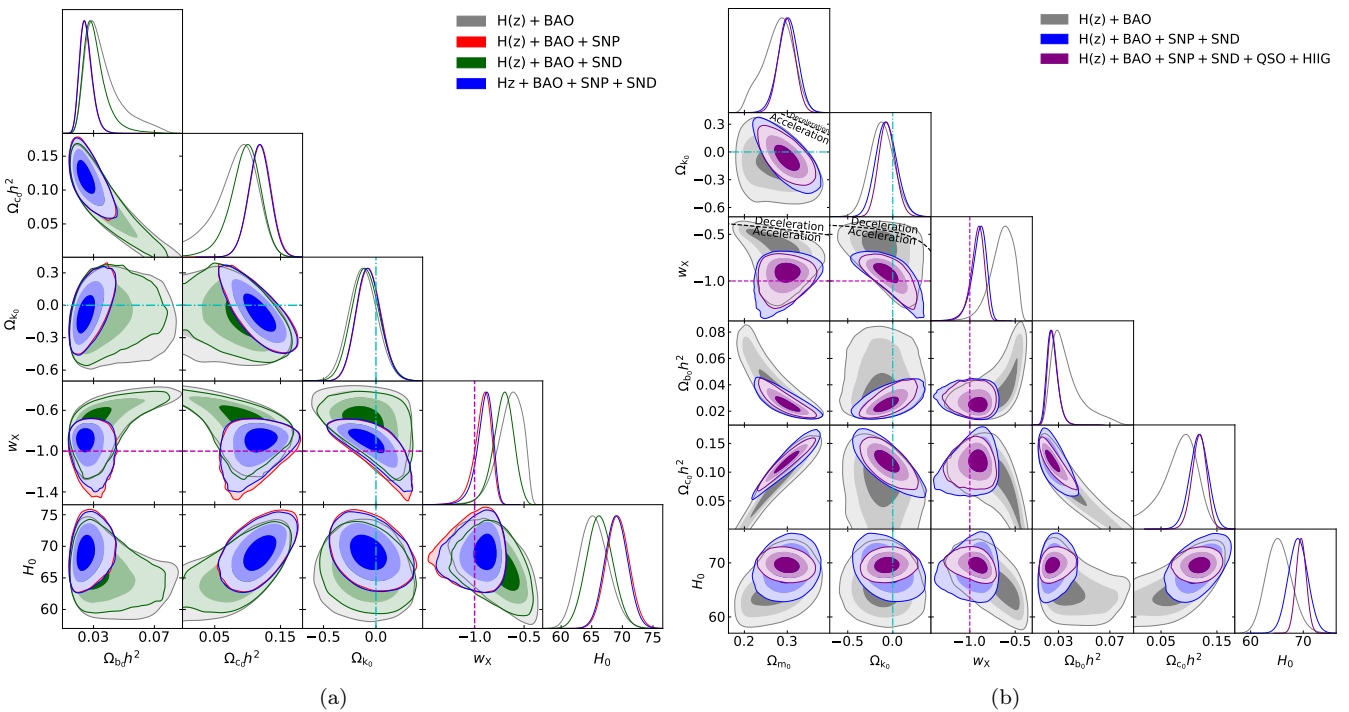


Figure 4. Same as Fig. 3 but for non-flat XCDM, where the zero acceleration lines in each of the three subpanels of the right panel are computed for the third cosmological parameter set to the $H(z) + \text{BAO}$ data best-fitting values listed in Table 2. Currently-accelerating cosmological expansion occurs below these lines. The cyan dash-dot lines represent the flat XCDM case, with closed spatial hypersurfaces either below or to the left. In all cases, almost all of the favored parameter space is associated with currently-accelerating cosmological expansion. The magenta lines indicate $w_X = -1$, i.e. the non-flat ΛCDM model.

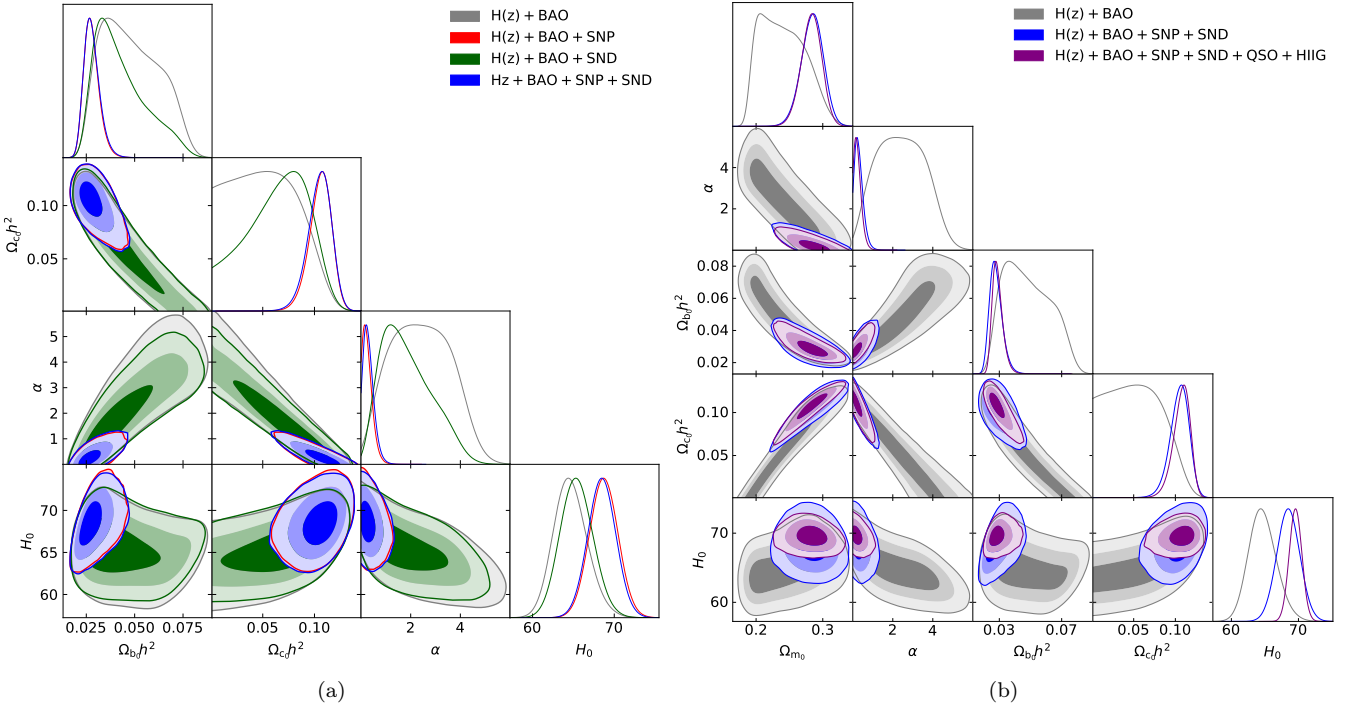


Figure 5. 1σ , 2σ , and 3σ confidence contours for flat ϕ CDM. In all cases, the favored parameter space is associated with currently-accelerating cosmological expansion. The $\alpha = 0$ axis is the flat Λ CDM model.

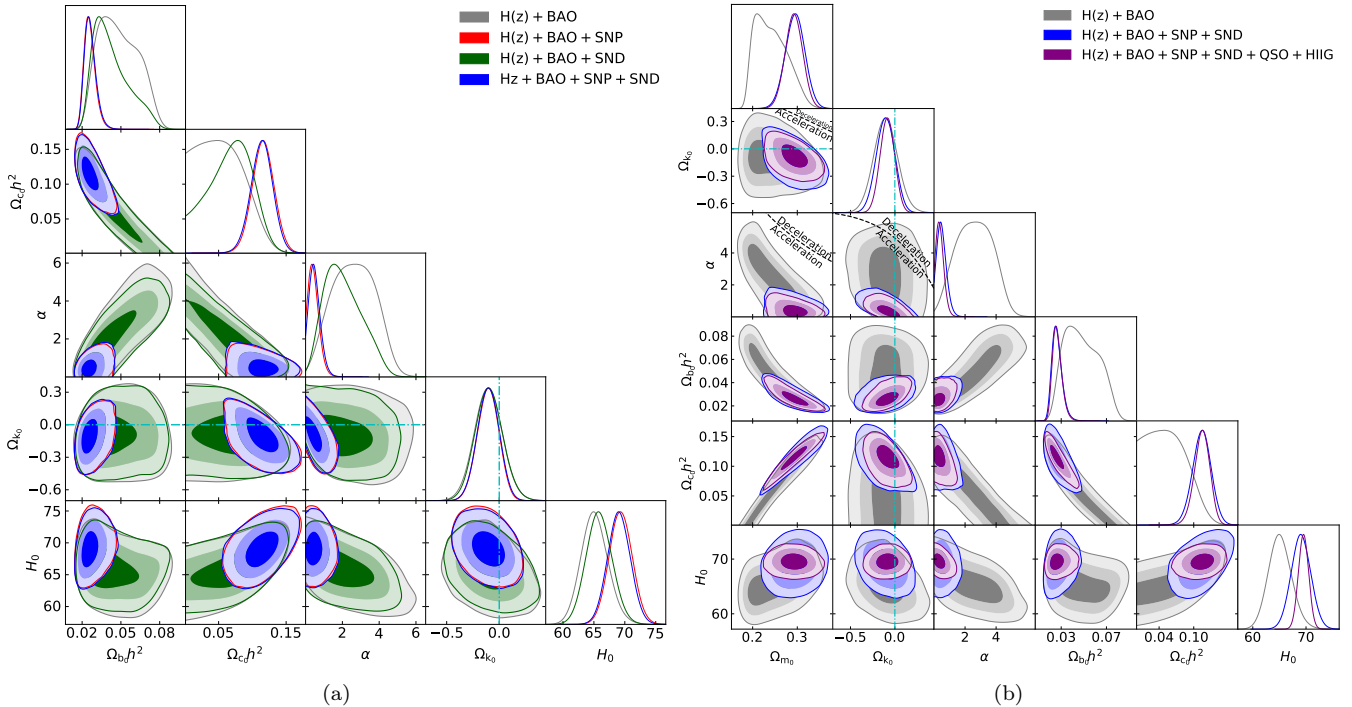


Figure 6. Same as Fig. 5 but for non-flat ϕ CDM, where the zero-acceleration lines in each of the sub-panels of the right panel are computed for the third cosmological parameter set to the $H(z) + \text{BAO}$ data best-fitting values listed in Table 2. Currently-accelerating cosmological expansion occurs below these lines. In all cases, almost all of the favored parameter space is associated with currently-accelerating cosmological expansion. The cyan dash-dot lines represent the flat ϕ CDM case, with closed spatial geometry either below or to the left. The $\alpha = 0$ axis is the non-flat Λ CDM model.

Table 3. One-dimensional marginalized best-fitting parameter values and uncertainties ($\pm 1\sigma$ error bars or 2σ limits) for all models from various combinations of data.

Model	Data set	$\Omega_{b0}h^2$	$\Omega_{c0}h^2$	Ω_{m0}	Ω_{k0}	w_X	α	H_0^a
Flat Λ CDM	$H(z) + \text{BAO}$	$0.0245^{+0.0026}_{-0.0032}$	0.1182 ± 0.0077	$0.298^{+0.015}_{-0.017}$	—	—	—	69.33 ± 1.75
	HzBSNP ^b	$0.0245^{+0.0025}_{-0.0031}$	0.1182 ± 0.0068	0.298 ± 0.013	—	—	—	69.32 ± 1.70
	HzBSND ^c	$0.0239^{+0.0025}_{-0.0032}$	0.1206 ± 0.0076	$0.305^{+0.015}_{-0.017}$	—	—	—	69.04 ± 1.74
	HzBSNPD ^d	$0.0241^{+0.0024}_{-0.0030}$	0.1199 ± 0.0067	0.303 ± 0.013	—	—	—	69.14 ± 1.68
	HzBSNPDQH ^e	$0.0253^{+0.0019}_{-0.0022}$	0.1202 ± 0.0057	0.299 ± 0.012	—	—	—	69.98 ± 0.91
Non-flat Λ CDM	$H(z) + \text{BAO}$	$0.0265^{+0.0035}_{-0.0059}$	0.1104 ± 0.0192	0.291 ± 0.024	$0.047^{+0.095}_{-0.112}$	—	—	68.71 ± 2.24
	HzBSNP ^b	$0.0253^{+0.0033}_{-0.0049}$	$0.1158^{+0.0161}_{-0.0160}$	0.296 ± 0.022	0.013 ± 0.073	—	—	69.22 ± 1.86
	HzBSND ^c	$0.0276^{+0.0038}_{-0.0062}$	$0.1049^{+0.0188}_{-0.0187}$	0.288 ± 0.024	$0.090^{+0.093}_{-0.106}$	—	—	67.92 ± 2.10
	HzBSNPD ^d	$0.0257^{+0.0033}_{-0.0050}$	0.1133 ± 0.0160	0.295 ± 0.022	0.032 ± 0.072	—	—	68.83 ± 1.82
	HzBSNPDQH ^e	$0.0260^{+0.0031}_{-0.0046}$	$0.1188^{+0.0138}_{-0.0123}$	0.297 ± 0.020	0.007 ± 0.063	—	—	69.95 ± 0.93
Flat XCDM	$H(z) + \text{BAO}$	$0.0372^{+0.0045}_{-0.0138}$	$0.0777^{+0.0351}_{-0.0182}$	$0.270^{+0.036}_{-0.022}$	—	$-0.688^{+0.174}_{-0.109}$	—	$65.22^{+2.21}_{-2.64}$
	HzBSNP ^b	$0.0261^{+0.0030}_{-0.0041}$	0.1118 ± 0.0105	0.292 ± 0.016	—	-0.951 ± 0.063	—	68.91 ± 1.76
	HzBSND ^c	$0.0331^{+0.0038}_{-0.0091}$	$0.0881^{+0.0235}_{-0.0137}$	$0.279^{+0.027}_{-0.019}$	—	$-0.739^{+0.110}_{-0.108}$	—	65.95 ± 2.08
	HzBSNPD ^d	$0.0264^{+0.0031}_{-0.0042}$	0.1105 ± 0.0107	0.292 ± 0.016	—	-0.932 ± 0.061	—	68.62 ± 1.73
	HzBSNPDQH ^e	$0.0273^{+0.0026}_{-0.0035}$	$0.1131^{+0.0104}_{-0.0095}$	0.291 ± 0.015	—	-0.949 ± 0.059	—	$69.67^{+0.97}_{-0.96}$
Non-flat XCDM	$H(z) + \text{BAO}$	$0.0367^{+0.0049}_{-0.0145}$	$0.0822^{+0.0376}_{-0.0233}$	$0.278^{+0.041}_{-0.030}$	$-0.122^{+0.137}_{-0.136}$	$-0.647^{+0.159}_{-0.084}$	—	$65.39^{+2.18}_{-2.59}$
	HzBSNP ^b	$0.0251^{+0.0031}_{-0.0049}$	0.1186 ± 0.0167	0.301 ± 0.023	$-0.066^{+0.111}_{-0.124}$	$-0.923^{+0.104}_{-0.060}$	—	69.24 ± 1.87
	HzBSND ^c	$0.0315^{+0.0039}_{-0.0091}$	$0.0956^{+0.0260}_{-0.0190}$	$0.290^{+0.031}_{-0.026}$	-0.099 ± 0.133	$-0.714^{+0.116}_{-0.089}$	—	66.30 ± 2.14
	HzBSNPD ^d	$0.0253^{+0.0032}_{-0.0048}$	$0.1178^{+0.0166}_{-0.0165}$	0.301 ± 0.023	$-0.071^{+0.110}_{-0.123}$	$-0.904^{+0.098}_{-0.058}$	—	69.00 ± 1.85
	HzBSNPDQH ^e	$0.0256^{+0.0030}_{-0.0046}$	$0.1182^{+0.0136}_{-0.0121}$	0.299 ± 0.020	$-0.063^{+0.087}_{-0.097}$	$-0.919^{+0.085}_{-0.056}$	—	69.59 ± 0.97
Flat ϕ CDM	$H(z) + \text{BAO}$	$0.0480^{+0.0113}_{-0.0193}$	$0.0524^{+0.0246}_{-0.0427}$	$0.240^{+0.024}_{-0.044}$	—	—	$2.418^{+1.197}_{-1.331}$	$64.67^{+1.86}_{-2.22}$
	HzBSNP ^b	$0.0278^{+0.0030}_{-0.0046}$	$0.1055^{+0.0119}_{-0.0091}$	0.284 ± 0.016	—	—	< 0.666	$68.71^{+1.73}_{-1.74}$
	HzBSND ^c	$0.0429^{+0.0071}_{-0.0170}$	$0.0641^{+0.0371}_{-0.0235}$	$0.251^{+0.038}_{-0.031}$	—	—	$1.863^{+0.674}_{-1.316}$	$65.41^{+1.91}_{-2.08}$
	HzBSNPD ^d	$0.0279^{+0.0031}_{-0.0048}$	$0.1047^{+0.0125}_{-0.0096}$	$0.284^{+0.017}_{-0.016}$	—	—	$0.320^{+0.108}_{-0.277}$	$68.48^{+1.71}_{-1.70}$
	HzBSNPDQH ^e	$0.0289^{+0.0025}_{-0.0040}$	$0.1073^{+0.0116}_{-0.0081}$	$0.283^{+0.016}_{-0.014}$	—	—	$0.261^{+0.067}_{-0.254}$	69.57 ± 0.94
Non-flat ϕ CDM	$H(z) + \text{BAO}$	$0.0482^{+0.0126}_{-0.0190}$	$0.0544^{+0.0194}_{-0.0497}$	$0.242^{+0.024}_{-0.046}$	-0.103 ± 0.132	—	$2.618^{+1.213}_{-1.226}$	$65.14^{+2.02}_{-2.29}$
	HzBSNP ^b	$0.0260^{+0.0033}_{-0.0051}$	$0.1159^{+0.0163}_{-0.0161}$	0.296 ± 0.022	-0.106 ± 0.102	—	$0.454^{+0.174}_{-0.372}$	69.33 ± 1.86
	HzBSND ^c	$0.0427^{+0.0076}_{-0.0177}$	$0.0670^{+0.0379}_{-0.0282}$	$0.253^{+0.037}_{-0.039}$	-0.097 ± 0.130	—	$2.058^{+0.779}_{-1.269}$	65.86 ± 2.09
	HzBSNPD ^d	$0.0264^{+0.0034}_{-0.0052}$	0.1139 ± 0.0161	0.295 ± 0.022	-0.105 ± 0.104	—	$0.509^{+0.212}_{-0.370}$	$69.06^{+1.84}_{-1.83}$
	HzBSNPDQH ^e	$0.0265^{+0.0031}_{-0.0048}$	$0.1142^{+0.0141}_{-0.0123}$	0.293 ± 0.020	-0.085 ± 0.081	—	$0.399^{+0.159}_{-0.313}$	69.53 ± 0.95

^a km s⁻¹ Mpc⁻¹.^b $H(z) + \text{BAO} + \text{SN-Pantheon}$.^c $H(z) + \text{BAO} + \text{SN-DES}$.^d $H(z) + \text{BAO} + \text{SN-Pantheon} + \text{SN-DES}$.^e $H(z) + \text{BAO} + \text{SN-Pantheon} + \text{SN-DES} + \text{QSO} + \text{H II G}$.

5.3 HzBSNPDQH constraints

Since the constraints derived from $H(z)$, BAO, SN-Pantheon, SN-DES, QSO, and H II G data are not inconsistent, in this subsection we jointly analyze HzBSNPDQH data to determine more restrictive constraints on the cosmological parameters (though as discussed in Sec. 5.4, we believe these constraints to be less reliable than those that stem from the HzSNPD combination, so we only describe the broad outlines here).

For flat Λ CDM, the error bars we derive for $\Omega_{b0}h^2$, $\Omega_{c0}h^2$, and Ω_{m0} are larger than the *Planck* error bars, though our central estimates of these quantities are broadly consistent with those derived from *Planck*. In a similar fashion, we find larger error bars on H_0 in flat Λ CDM than does *Planck*, though our central estimate is higher than theirs. Generally, the constraints we derive on H_0 are more consistent with the

median statistics estimate of $H_0 = 68 \pm 2.8$ km s⁻¹ Mpc⁻¹ (Chen & Ratra 2011), than with the local Hubble constant measurement of $H_0 = 74.03 \pm 1.42$ km s⁻¹ Mpc⁻¹ (Riess et al. 2019).

We find mild evidence for spatial curvature, with non-flat XCDM and ϕ CDM favoring closed geometry, and non-flat Λ CDM mildly favoring open geometry. The constraints from non-flat Λ CDM and XCDM are consistent with spatially flat hypersurfaces to within less than 1σ . Additionally, we find mild evidence for dark energy dynamics, with the best-fitting value of w_X being 0.86σ (1.45σ) away from $w_X = -1$ in flat (non-flat) XCDM, and the best-fitting value of α being 1.03σ (1.27σ) away from $\alpha = 0$ in flat (non-flat) ϕ CDM.

5.4 Model comparison

The values of $\Delta\chi^2$, ΔAIC , ΔBIC , and the reduced χ^2 (χ^2/ν) are reported in Table 4, where $\Delta\chi^2$, ΔAIC , and ΔBIC , respectively, are defined as the differences between the values of the χ^2 , AIC , and BIC for a given model and their corresponding minimum values among all models. From Table 4, we see that the reduced χ^2 values determined from the $H(z) + \text{BAO}$ data combination range from 0.49 to 0.62, which is probably due to the $H(z)$ data having overestimated error bars (see Cao et al. 2021 for discussions of the systematic errors of these data). As discussed in Ryan et al. (2019) and Cao et al. (2020), the underestimated systematic uncertainties in QSO and H II G data¹² result in larger reduced χ^2 (~ 1.34) for the models in the HzBSNPDQH case. The reduced χ^2 values for the HzBSNP and HzBSNP cases are around unity for all models and for the HzBSND case range from 0.77 to 0.87. Of the combinations we study here, on the basis of these reduced χ^2 values, the HzBSNPD constraints should be viewed as the most reliable ones.

We find that based on the AIC and BIC , flat ΛCDM and flat ϕCDM are the most favored models in different data combination cases. The ΔAIC results show that the most favored model is flat ΛCDM in the HzBSNP case, while the most favored model is flat ϕCDM in the rest of the data combinations. The ΔBIC results show that the most favored model is flat ϕCDM in the $H(z) + \text{BAO}$ and HzBSND cases, and is flat ΛCDM in the remaining cases. For both ΔAIC and ΔBIC results, the most disfavored model is non-flat ΛCDM in the $H(z) + \text{BAO}$ and HzBSND cases, and is non-flat XCDM in all other cases, with positive evidence against non-flat ΛCDM and either positive or very strong evidence (depending on the data combination) against non-flat XCDM.

Overall, the ΔAIC results show no strong evidence against any model, and neither do the ΔBIC results for the $H(z) + \text{BAO}$ and HzBSND cases. However, in the HzBSNP and HzBSNPDQH cases, the ΔBIC results show strong evidence against the non-flat ΛCDM and flat XCDM models, and very strong evidence against the non-flat ϕCDM and XCDM models. In the HzBSNPD case, the evidence against flat XCDM and flat ϕCDM is positive, the evidence against non-flat ΛCDM is strong, and the evidence against non-flat ϕCDM and non-flat XCDM is very strong. Based on the $\Delta\chi^2$ results, non-flat ϕCDM has the minimum χ^2 in all cases.

In summary, the HzBSNPD data favor flat ϕCDM (AIC) or flat ΛCDM (BIC) among the six models we study here.

6 CONCLUSION

By analyzing a total of 1383 measurements, consisting of 31 $H(z)$, 11 BAO, 1048 SN-Pantheon, 20 SN-DES, 120 QSO, and 153 H II G data points, we jointly constrain cosmological parameters in six flat and non-flat cosmological models.

From the constraints derived using the cosmological

¹² Roberto Terlevich and his colleagues are currently investigating the systematic uncertainties of the H II G data, the results of which they plan to publish in a future paper (Roberto Terlevich, private communication, 2021).

models, we can identify some relatively model-independent features. As discussed in Sec. 5.4, the $H(z) + \text{BAO} + \text{SN-Pantheon} + \text{SN-DES}$ (HzBSNPD) data combination produces the most reliable constraints. In particular, for the HzBSNPD data combination, we find a reasonable and fairly restrictive summary value of $\Omega_{m0} = 0.294 \pm 0.020$,¹³ which is in good agreement with many other recent measurements (e.g. 0.315 ± 0.007 from Planck Collaboration 2020). A fairly restrictive summary value of $H_0 = 68.8 \pm 1.8 \text{ km s}^{-1} \text{ Mpc}^{-1}$ is found to be in better agreement with the estimates of Chen & Ratra (2011) and Planck Collaboration (2020) than with the measurement of Riess et al. (2019); note that the constraints from BAO data do not depend on physics of the early Universe (with $\Omega_{b0}h^2$ being a free parameter that is fitted to the data used here). There is some room for dark energy dynamics or a little spatial curvature energy density in the HzBSNPD constraints, but based on AIC and BIC criteria, flat ϕCDM or flat ΛCDM are the best candidate models.

ACKNOWLEDGEMENTS

We thank Javier de Cruz Pérez for useful discussions on the data. This work was partially funded by Department of Energy grant DE-SC0011840. The computing for this project was performed on the Beocat Research Cluster at Kansas State University, which is funded in part by NSF grants CNS-1006860, EPS-1006860, EPS-0919443, ACI-1440548, CHE-1726332, and NIH P20GM113109.

DATA AVAILABILITY

The H II G data used in this article were provided to us by the authors of González-Morán et al. (2019). These data will be shared on request to the corresponding author with the permission of the authors of González-Morán et al. (2019).

REFERENCES

- Abbassi M. H., Abbassi A. H., 2020, *J. Cosmology Astropart. Phys.*, **2020**, 042
- Agudelo Ruiz J. A., Fabris J. C., Velasquez-Toribio A. M., Shapiro I. L., 2020, *Gravitation and Cosmology*, **26**, 316
- Alam S., et al., 2017, *MNRAS*, **470**, 2617
- Ata M., et al., 2018, *MNRAS*, **473**, 4773
- Aubourg É., et al., 2015, *Phys. Rev. D*, **92**, 123516
- Avsajanishvili O., Samushia L., Arkhipova N. A., Kahnashvili T., 2015, preprint, ([arXiv:1511.09317](https://arxiv.org/abs/1511.09317))
- Birrer S., et al., 2020, *A&A*, **643**, A165
- Blum K., Castorina E., Simonović M., 2020, *ApJ*, **892**, L27
- Bonga B., Gupt B., Yokomizo N., 2016, *J. Cosmology Astropart. Phys.*, **2016**, 031
- Borah S. S., Hudson M. J., Lavaux G., 2020, preprint, ([arXiv:2010.01119](https://arxiv.org/abs/2010.01119))

¹³ Here we take the summary central value to be the mean of the two of six central-most values. As for the uncertainty, we call the difference between the two central-most values twice the systematic uncertainty and the average of the two central-most error bars the statistical uncertainty, and compute the summary error bar as the quadrature sum of the two uncertainties.

Table 4. $\Delta\chi^2$, ΔAIC , ΔBIC , and χ^2_{\min}/ν values.

Quantity	Data set	Flat Λ CDM	Non-flat Λ CDM	Flat XCDM	Non-flat XCDM	Flat ϕ CDM	Non-flat ϕ CDM
$\Delta\chi^2$	$H(z) + \text{BAO}$	5.48	5.42	1.49	0.15	1.32	0.00
	HzBSNP ^a	2.91	2.91	2.32	1.51	1.15	0.00
	HzBSND ^b	6.74	6.19	1.37	0.25	1.08	0.00
	HzBSNPD ^c	3.33	3.22	2.10	1.23	1.05	0.00
ΔAIC	HzBSNPDQH ^d	2.99	2.99	2.27	1.25	0.95	0.00
	$H(z) + \text{BAO}$	2.16	4.10	0.17	0.83	0.00	0.68
	HzBSNP ^a	0.00	2.00	1.41	2.60	0.24	1.09
	HzBSND ^b	3.66	5.11	0.29	1.17	0.00	0.92
	HzBSNPD ^c	0.28	2.17	1.05	2.18	0.00	0.95
ΔBIC	HzBSNPDQH ^d	0.04	2.04	1.32	2.30	0.00	1.05
	$H(z) + \text{BAO}$	0.43	4.10	0.17	2.57	0.00	2.42
	HzBSNP ^a	0.00	6.99	6.40	12.58	5.23	11.07
	HzBSND ^b	1.53	5.11	0.29	3.30	0.00	3.04
χ^2_{\min}/ν	HzBSNPD ^c	0.00	6.90	5.78	11.92	4.72	10.69
	HzBSNPDQH ^d	0.00	7.23	6.51	12.72	5.19	11.47
	$H(z) + \text{BAO}$	0.61	0.62	0.52	0.49	0.51	0.49
	HzBSNP ^a	0.97	0.97	0.97	0.97	0.97	0.97
χ^2_{\min}/ν	HzBSND ^b	0.86	0.87	0.78	0.78	0.78	0.77
	HzBSNPD ^c	0.98	0.98	0.98	0.98	0.97	0.97
	HzBSNPDQH ^d	1.34	1.34	1.34	1.34	1.34	1.34

^a $H(z) + \text{BAO} + \text{SN-Pantheon}$.^b $H(z) + \text{BAO} + \text{SN-DES}$.^c $H(z) + \text{BAO} + \text{SN-Pantheon} + \text{SN-DES}$.^d $H(z) + \text{BAO} + \text{SN-Pantheon} + \text{SN-DES} + \text{QSO} + \text{H II G}$.

- Breuval L., et al., 2020, [A&A, 643, A115](#)
- Campanelli L., Fogli G. L., Kahnashvili T., Marrone A., Ratra B., 2012, [European Physical Journal C, 72, 2218](#)
- Cao S., Zheng X., Biesiada M., Qi J., Chen Y., Zhu Z.-H., 2017, [A&A, 606, A15](#)
- Cao S., Ryan J., Ratra B., 2020, [MNRAS, 497, 3191](#)
- Cao S., Ryan J., Khadka N., Ratra B., 2021, [MNRAS, 501, 1520](#)
- Carter P., Beutler F., Percival W. J., Blake C., Koda J., Ross A. J., 2018, [MNRAS, 481, 2371](#)
- Chávez R., Terlevich R., Terlevich E., Bresolin F., Melnick J., Plionis M., Basilakos S., 2014, [MNRAS, 442, 3565](#)
- Chen G., Ratra B., 2011, [PASP, 123, 1127](#)
- Chen G., Gott III J. R., Ratra B., 2003, [PASP, 115, 1269](#)
- Chen Y., Ratra B., Biesiada M., Li S., Zhu Z.-H., 2016, [ApJ, 829, 61](#)
- Chen Y., Kumar S., Ratra B., 2017, [ApJ, 835, 86](#)
- Coley A. A., Ellis G. F. R., 2020, [Classical and Quantum Gravity, 37, 013001](#)
- Conley A., et al., 2011, [ApJS, 192, 1](#)
- Cuceu A., Farr J., Lemos P., Font-Ribera A., 2019, [J. Cosmology Astropart. Phys., 2019, 044](#)
- DES Collaboration 2018, [MNRAS, 480, 3879](#)
- DES Collaboration 2019a, [Phys. Rev. D, 99, 123505](#)
- DES Collaboration 2019b, [MNRAS, 483, 4866](#)
- DES Collaboration 2019c, [ApJ, 872, L30](#)
- DES Collaboration 2019d, [ApJ, 874, 150](#)
- Deng H.-K., Wei H., 2018, [European Physical Journal C, 78, 755](#)
- Denzel P., Coles J. P., Saha P., Williams L. L. R., 2021, [MNRAS, 501, 784](#)
- Dhawan S., Jha S. W., Leibundgut B., 2018, [A&A, 609, A72](#)
- Di Valentino E., Melchiorri A., Silk J., 2020, [Nature Astronomy, 4, 196](#)
- Di Valentino E., Melchiorri A., Silk J., 2021, [ApJ, 908, L9](#)
- Domínguez A., et al., 2019, [ApJ, 885, 137](#)
- du Mas des Bourboux H., et al., 2020, [ApJ, 901, 153](#)
- eBOSS Collaboration 2020, preprint, ([arXiv:2007.08991](#))
- Efstathiou G., 2020, preprint, ([arXiv:2007.10716](#))
- Efstathiou G., Gratton S., 2020, [MNRAS, 496, L91](#)
- Farooq O., Mania D., Ratra B., 2015, [Ap&SS, 357, 11](#)
- Farooq O., Ranjeet Madiyar F., Crandall S., Ratra B., 2017, [ApJ, 835, 26](#)
- Fernández Arenas D., et al., 2018, [MNRAS, 474, 1250](#)
- Foreman-Mackey D., Hogg D. W., Lang D., Goodman J., 2013, [PASP, 125, 306](#)
- Freedman W. L., et al., 2020, [ApJ, 891, 57](#)
- Gao C., Chen Y., Zheng J., 2020, [Research in Astronomy and Astrophysics, 20, 151](#)
- Geng C.-Q., Hsu Y.-T., Yin L., Zhang K., 2020, [Chinese Physics C, 44, 105104](#)
- Gómez-Valent A., Amendola L., 2018, [J. Cosmology Astropart. Phys., 4, 051](#)
- González-Morán A. L., et al., 2019, [MNRAS, 487, 4669](#)
- Gott III J. R., Vogeley M. S., Podariu S., Ratra B., 2001, [ApJ, 549, 1](#)
- Handley W., 2019, [Phys. Rev. D, 100, 123517](#)
- Handley W., 2021, [Phys. Rev. D, 103, L041301](#)
- Harvey D., 2020, [MNRAS, 498, 2871](#)
- Jesus J. F., Valentim R., Moraes P. H. R. S., Malheiro M., 2021, [MNRAS, 500, 2227](#)
- Khadka N., Ratra B., 2020a, [MNRAS, 492, 4456](#)
- Khadka N., Ratra B., 2020b, [MNRAS, 497, 263](#)
- Khadka N., Ratra B., 2020c, [MNRAS, 499, 391](#)
- Khadka N., Ratra B., 2021, [MNRAS, Khetan N., et al., 2021, A&A, 647, A72](#)
- Kim Y. J., Kang J., Lee M. G., Jang I. S., 2020, [ApJ, 905, 104](#)
- Kumar D., Jain D., Mahajan S., Mukherjee A., Rani N., 2021, [Phys. Rev. D, 103, 063511](#)
- Lesgourges J., Tram T., 2014, [J. Cosmology Astropart. Phys., 2014, 032](#)
- Lewis A., 2019, preprint, ([arXiv:1910.13970](#))

- Li E.-K., Du M., Xu L., 2020, *MNRAS*, **491**, 4960
 Lin W., Ishak M., 2019, preprint, ([arXiv:1909.10991](#))
 Lucchin F., Matarrese S., 1985, *Phys. Rev. D*, **32**, 1316
 Lyu M.-Z., Haridasu B. S., Viel M., Xia J.-Q., 2020, *ApJ*, **900**, 160
 Martin J., 2012, *Comptes Rendus Physique*, **13**, 566
 Martinelli M., Tutzus I., 2019, *Symmetry*, **11**, 986
 Ooba J., Ratra B., Sugiyama N., 2018a, *ApJ*, **864**, 80
 Ooba J., Ratra B., Sugiyama N., 2018b, *ApJ*, **866**, 68
 Ooba J., Ratra B., Sugiyama N., 2018c, *ApJ*, **869**, 34
 Ooba J., Ratra B., Sugiyama N., 2019, *Ap&SS*, **364**, 176
 Park C.-G., Ratra B., 2018, *ApJ*, **868**, 83
 Park C.-G., Ratra B., 2019a, *Ap&SS*, **364**, 82
 Park C.-G., Ratra B., 2019b, *Ap&SS*, **364**, 134
 Park C.-G., Ratra B., 2019c, *ApJ*, **882**, 158
 Park C.-G., Ratra B., 2020, *Phys. Rev. D*, **101**, 083508
 Pavlov A., Westmoreland S., Saaidi K., Ratra B., 2013, *Phys. Rev. D*, **88**, 123513
 Peebles P. J. E., 1984, *ApJ*, **284**, 439
 Peebles P. J. E., Ratra B., 1988, *ApJ*, **325**, L17
 Philcox O. H. E., Ivanov M. M., Simonović M., Zaldarriaga M., 2020, *J. Cosmology Astropart. Phys.*, **2020**, 032
 Planck Collaboration 2020, *A&A*, **641**, A6
 Pogosian L., Zhao G.-B., Jedamzik K., 2020, *ApJ*, **904**, L17
 Rameez M., Sarkar S., 2019, preprint, ([arXiv:1911.06456](#))
 Rana A., Jain D., Mahajan S., Mukherjee A., 2017, *J. Cosmology Astropart. Phys.*, **3**, 028
 Ratra B., 1989, *Phys. Rev. D*, **40**, 3939
 Ratra B., 2017, *Phys. Rev. D*, **96**, 103534
 Ratra B., Peebles P. J. E., 1988, *Phys. Rev. D*, **37**, 3406
 Ratra B., Peebles P. J. E., 1995, *Phys. Rev. D*, **52**, 1837
 Ratra B., Vogeley M. S., 2008, *PASP*, **120**, 235
 Riess A. G., 2019, *Nature Reviews Physics*, **2**, 10
 Riess A. G., Casertano S., Yuan W., Macri L. M., Scolnic D., 2019, *ApJ*, **876**, 85
 Rigault M., et al., 2015, *ApJ*, **802**, 20
 Ryan J., Doshi S., Ratra B., 2018, *MNRAS*, **480**, 759
 Ryan J., Chen Y., Ratra B., 2019, *MNRAS*, **488**, 3844
 Samushia L., Dev A., Jain D., Ratra B., 2010, *Physics Letters B*, **693**, 509
 Sangwan A., Tripathi A., Jassal H. K., 2018, preprint, ([arXiv:1804.09350](#))
 Schöneberg N., Lesgourgues J., Hooper D. C., 2019, *J. Cosmology Astropart. Phys.*, **2019**, 029
 Scolnic D. M., et al., 2018, *ApJ*, **859**, 101
 Singh A., Sangwan A., Jassal H. K., 2019, *J. Cosmology Astropart. Phys.*, **2019**, 047
 Solà Peracaula J., de Cruz Pérez J., Gómez-Valent A., 2018, *MNRAS*, **478**, 4357
 Solà Peracaula J., Gómez-Valent A., de Cruz Pérez J., 2019, *Physics of the Dark Universe*, **25**, 100311
 Solà J., Gómez-Valent A., de Cruz Pérez J., 2017, *Modern Physics Letters A*, **32**, 1750054
 Thavanesan A., Werth D., Handley W., 2021, *Phys. Rev. D*, **103**
 Ureña-López L. A., Roy N., 2020, *Phys. Rev. D*, **102**, 063510
 Vagnozzi S., Di Valentino E., Gariazzo S., Melchiorri A., Mena O., Silk J., 2020, preprint, ([arXiv:2010.02230](#))
 Vagnozzi S., Loeb A., Moresco M., 2021, *ApJ*, **908**, 84
 Velásquez-Toribio A. M., Fabris J. C., 2020, *European Physical Journal C*, **80**, 1210
 Wei J.-J., 2018, *ApJ*, **868**, 29
 Yang Y., Gong Y., 2020, preprint, ([arXiv:2007.05714](#))
 Yashar M., Bozek B., Abrahamse A., Albrecht A., Barnard M., 2009, *Phys. Rev. D*, **79**, 103004
 Yu H., Ratra B., Wang F.-Y., 2018, *ApJ*, **856**, 3
 Zeng H., Yan D., 2019, *ApJ*, **882**, 87
 Zhai Z., Blanton M., Slosar A., Tinker J., 2017, *ApJ*, **850**, 183
 Zhang X., Huang Q.-G., 2021, *Phys. Rev. D*, **103**, 043513

Zhang B. R., Childress M. J., Davis T. M., Karpenka N. V., Lidman C., Schmidt B. P., Smith M., 2017, *MNRAS*, **471**, 2254

This paper has been typeset from a *T_EX/L_AT_EX* file prepared by the author.